# Algorithm for Modeling Dual-Polarized MIMO Channel in Land Mobile Satellite Communications

Xin Wang and Chenhao Qi
School of Information Science and Engineering
Southeast University, Nanjing 210096, China
Email: qch@seu.edu.cn

***Abstract*—The channel factors during signal propagation from the satellite to moving user terminal (UT) is comprehensively analyzed. Then an algorithm is presented to model dual-polarized MIMO LMS channel, which investigates almost all channel factors including temporal and polarization correlation, line-of-sight (LOS) shadowing, multipath effect, cross-polar discrimination (XPD) of antennas, cross-polar coupling (XPC) of environments, elevation angle, user environments and Doppler frequency shift. An algorithm table embedded with outer-loop iterations and inner-loop iterations is given to generate the dual-polarized MIMO LMS channel. Simulation results show that compared with single-input single-output (SISO) LMS system, MIMO LMS system can respectively achieve the improvement of 66%, 60% and 54% in terms of 1% outage capacity at signal-to-noise ratio (SNR) of 20dB in open, suburban and urban environment.**

***Index Terms*—Land mobile satellite (LMS), multi-input multi-output (MIMO), dual polarization, channel model**

## I. Introduction

The appealing performance improvement achieved by multi-input multi-output (MIMO) technique in terrestrial wireless systems promotes its application on land mobile satellite (LMS) communications [1]. However, different to terrestrial wireless channel, the LMS channel is characterized by a strong line-of-sight (LOS) component without rich scatterers. Therefore, the MIMO channel matrix in LMS system is usually rank deficient due to the highly correlated propagation paths [2], [3]. To solve this problem, polarization diversity is adopted [4], [5]. The statistical model for dual-polarized MIMO LMS channel at S band are given in [5]. However, it only considers the low elevation angle, which is not appropriate for the practical LMS system. In [6], larger elevation angle is further considered for dual-polarized MIMO LMS system. However, it does not take the Doppler frequency shift caused by the moving user terminal (UT) into account.

In this paper, we first analyze the channel factors during signal propagation from the satellite to the moving UT. Then we present an algorithm for modeling dual-polarized MIMO LMS channel, which comprehensively investigates almost all factors, including temporal and polarization correlation, LOS shadowing, multipath effect, cross-polar discrimination (XPD) of antennas, cross-polar coupling (XPC) of environments, elevation angle, user environments and Doppler frequency shift. An algorithm table embedded with outer-loop iterations and inner-loop iterations is given to generate the dual-polarized MIMO LMS channel. Simulation results show that compared with single-input single-output (SISO) LMS system, MIMO LMS system can respectively achieve the improvement of 66%, 60% and 54% in terms of 1% outage capacity at signal-to-noise ratio (SNR) of 20dB in open, suburban and urban environment.

The notations used in this paper are defined as follows: Symbols for matrices (upper case) and vectors (lower case) are in boldface. $(\cdot)^T$, $(\cdot)^H$, $\otimes$, $\odot$, $U$, $\mathcal{N}$, $\mathcal{CN}$, $\mathbf{0}^M$, $\boldsymbol{I}_L$ denote the transpose, the conjugate transpose (Hermitian), Kronecker product operator, entrywise product of matrices, the uniformly distribution, the Gaussian random distribution, the complex Gaussian random distribution, the zero vector of size $M$, and the identity matrix of size $L$, respectively. The operator round$(x)$ rounds $x$ to the nearest integer. The operator vec$(\boldsymbol{A})$ denotes the vectorization of the matrix $\boldsymbol{A}$.

## II. System model of dual-polarized MIMO LMS channel

The diagram of the dual-polarized MIMO LMS system is shown in Fig. 1. Each satellite and UT are equipped with an antenna using both right-hand circular polarization (RHCP) and left-hand circular polarization (LHCP). Then, the MIMO channel can be expressed by a $2\times2$ channel matrix $\boldsymbol{H} \triangleq [h_{ij}](i,j \in \{1,2\})$, where $h_{ij}$ is the gain between the $j$-th polarized channel on the satellite and the $i$-th polarized channel on the UT. The distribution for the envelope of $h_{ij}$, denoted as $|h_{ij}|$, is assumed to be the Loo distribution since it has already been extensively used and validated in DVB-SH standards. According to the Loo distribution, $\boldsymbol{H} = \overline{\boldsymbol{H}} + \widetilde{\boldsymbol{H}}$ is consisted of a large-scale fading component $\overline{\boldsymbol{H}} \triangleq [\overline{h}_{ij}](i,j \in \{1,2\})$ and a small-scale fading component $\widetilde{\boldsymbol{H}} \triangleq [\widetilde{h}_{ij}](i,j \in \{1,2\})$, representing the LOS shadowing and multipath diffuse respectively. We further denote

$$\overline{h}_{ij} = |\overline{h}_{ij}|e^{j\overline{\phi}_{ij}} \tag{1}$$

and

$$\widetilde{h}_{ij} = |\widetilde{h}_{ij}|e^{j\widetilde{\phi}_{ij}}, \tag{2}$$

where $|\overline{h}_{ij}|$ and $\overline{\phi}_{ij}$ are the envelope and phase of large-scale fading component $\overline{h}_{ij}$, $|\tilde{h}_{ij}|$ and $\tilde{\phi}_{ij}$ are the envelope and phase of small-scale fading component $\widetilde{h}_{ij}$. $|\overline{h}_{ij}|$ and $|\tilde{h}_{ij}|$ obey the log-normal distribution and the Rayleigh distribution, respectively. $\overline{\phi}_{ij}$ and $\tilde{\phi}_{ij}$ are independently and uniformly

978-1-5386-2062-5/17/$31.00 ©2017 IEEE

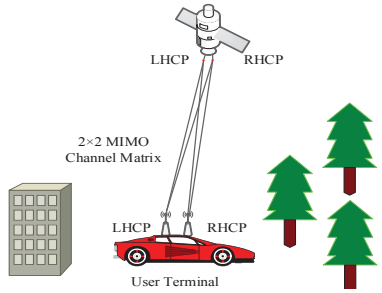


Fig. 1. System model of dual-polarized MIMO LMS channel.

distributed over $[0, 2\pi]$. To simplify the notations, we denote $r \triangleq |h_{ij}|$. The probability density function of $r$ is

$$p(r) = \frac{r}{b_0\sqrt{2\pi d_0}} \int_0^\infty \frac{1}{z} e^{-\frac{(\ln z-\mu)^2}{2d_0} - \frac{r^2+z^2}{2b_0}} I_0\left(\frac{rz}{b_0}\right) dz, \quad (3)$$

where $I_0(\cdot)$ is the zeroth order modified Bessel function. According to the convention, we denote $\alpha = 20\log_{10}(e^{\mu})$ and $\psi = 20\log_{10}(e^{\sqrt{d_0}})$ as the the mean and standard deviation of $|\overline{h}_{ij}|$ in the unit of dB. We denote $MP = 10\log_{10}(2b_0)$ as the average power of $|\tilde{h}_{ij}|$ in the unit of dB. Experimental datasets of $\alpha$, $\psi$ and $MP$ are provided in [7].

## III. Analysis of Several Effects on Dual-Polarized MIMO LMS Channel

### A. Temporal correlation

The temporal correlation is introduced by the movement of UT at a certain speed $v$. The temporal variation of LMS channel is modeled as a three-sate Markov random process with given state transition probability matrix $\boldsymbol{P}$ and state probability vector $\boldsymbol{w}$ [7]. The three states are denoted as $S_1$, $S_2$ and $S_3$, where $S_1$ indicates the LOS propagation, $S_2$ indicates the moderate fading, and $S_3$ indicates the deep fading. $p_{ij}$ denotes the transition probability from $S_i$ to $S_j$. The minimum duration of each state is denoted as $L_f/v$, where $L_f$ is a measurement in distance, i.e., state correlation distance. $L_f$ is usually set to be $3-8$ m [8]. The parameters of Loo distribution including $\alpha$, $\psi$ and $MP$ are assumed constant during each state.

The temporal correlation of small-scale fading components can be measured by correlation distance denoted as $L_m$, meaning that the small-scale fading components are randomly generated after the UT moves every $L_m$ meters. We usually set $L_m = \lambda/F$, where $\lambda$ is the signal wavelength and $F$ is a factor set to be $8-10$.

One method to introduce temporal correlation to large-scale fading components is the use of an infinite impulse response (IIR) filter [6]. The detailed procedures are listed as follows. First we generate Gaussian random uncorrelated samples $\{x_n, n = 1, 2, \ldots, M\}$ with zero mean and unit variance, where $M \triangleq \text{round}(L_f/L_m)$. Then we let these samples pass through a low-pass IIR filter to introduce temporal correlation. The IIR filter is described as

$$y_n = x_n + A \cdot y_{n-1}, \quad (4)$$

where $A = e^{-vT/L_d}$. $T = \lambda/(Fv)$ is the sampling interval, where $L_d$ is the correlation distance for large-scale fading components [8] . In order to maintain the variance of samples after filtering, $\{y_n, n = 1, 2, \ldots, M\}$ needs to multiply $\sqrt{1-A^2}$ in amplitude.

### B. Doppler effect

Due to the movement of the UT, the spectrum of the received signal will be affected by Doppler shift. In this case, a low-pass Butterworth filter can be used to introduce the Doppler shift for small-scale fading components [8]. The Butterworth filter's amplitude squared function is

$$|H_{\text{buff}}(f)|^2 = \frac{B}{1+(f/f_c)^{2k}}, \quad (5)$$

where $f_c$ is the cutoff frequency and $k$ is the order of the filter. As the signal variance will change after filtering, the multiplicative constant $B$ is used.

The phase of large-scale fading components are assumed to be linearly increased by a constant phase given by

$$\Delta\phi = 2\pi\frac{\cos\theta}{F} \quad (6)$$

when the UT travels every $L_m$ meters, where $\theta$ is the elevation angle.

### C. Cross-polarization discrimination effect

The cross-polarization discrimination (XPD) of satellite antenna is usually assumed to be infinity [6]. Thus we only consider XPD of UT antenna, denoted as $XPD_{ant}$. The power of large-scale fading and small-scale fading components is respectively given by

$$E\left\{|\overline{h}_{ij}|^2\right\} = \begin{cases} (\psi^2+\alpha^2)(1-\beta_{ant}) & i=j \\ (\psi^2+\alpha^2)\beta_{ant} & i\neq j \end{cases} \quad (7)$$

and

$$E\left\{|\tilde{h}_{ij}|^2\right\} = \begin{cases} MP(1-\gamma) & i=j \\ MP\gamma & i\neq j \end{cases}, \quad (8)$$

where $i, j \in \{1, 2\}$. Note that $\alpha$, $\psi$ and $MP$ are in linear scale instead of logarithmic scale. We denote cross-polarization coupling (XPC) of the propagation environment as $XPC_{env}$. $\beta_{ant}$ and $\gamma$, which are required for the computation of (7) and (8), are related to $XPD_{ant}$ and $XPC_{env}$ with the following three equations as

$$XPD_{ant} = 10\log_{10}\frac{1-\beta_{ant}}{\beta_{ant}}, \quad (9)$$

$$XPC_{env} = 10\log_{10}\frac{1-\gamma_{env}}{\gamma_{env}}, \quad (10)$$

$$\gamma = \beta_{ant}(1-\gamma_{env}) + (1-\beta_{ant})\gamma_{env}. \quad (11)$$

Some practical values of $XPD_{ant}$ and $XPC_{env}$ based on extensive measurements are provided in [5], [9].

### D. Polarization correlation

*1) Polarization correlation of large-scale fading components:*

Given a $2 \times 2$ channel matrix $|\overline{\boldsymbol{H}}|_w$ where each entry of $|\overline{\boldsymbol{H}}|_w$ independently obeying Gaussian distribution with zero mean and unit variance, we introduce the polarization correlation to $|\overline{\boldsymbol{H}}|_w$ by

$$\text{vec}\left(|\overline{\boldsymbol{H}}|_c\right) = \overline{\boldsymbol{C}}^{1/2} \cdot \text{vec}\left(|\overline{\boldsymbol{H}}|_w\right), \tag{12}$$

where $\overline{\boldsymbol{C}}$ is defined to be a $4 \times 4$ positive semidefinite Hermitian matrix to represent the covariance for $\overline{h}_{ij}$ [10]. The measurement data of $\overline{\boldsymbol{C}}$ in certain environment are given in [5].

Then we can generate $|\overline{\boldsymbol{H}}_{\text{LN}}|$ by

$$\text{vec}\left(|\overline{\boldsymbol{H}}_{\text{LN}}|\right) = 10^{\text{vec}\left[(|\overline{\boldsymbol{H}}|_c)\cdot\left(\frac{\psi}{20}\right)+\frac{\alpha}{20}\right]}. \tag{13}$$

*2) Polarization correlation of small-scale fading components:*

Given a $2 \times 2$ channel matrix $\widetilde{\boldsymbol{H}}_w$ where each entry of $\widetilde{\boldsymbol{H}}_w$ independently obeying complex Gaussian distribution with zero mean and unit variance, we introduce the polarization correlation to $\widetilde{\boldsymbol{H}}_w$ by

$$\text{vec}\left(\widetilde{\boldsymbol{H}}_c\right) = \widetilde{\boldsymbol{C}}^{1/2} \cdot \text{vec}\left(\widetilde{\boldsymbol{H}}_w\right), \tag{14}$$

where $\widetilde{\boldsymbol{C}}$ is defined to be a $4 \times 4$ positive semidefinite Hermitian matrix to represent the covariance for $\tilde{h}_{ij}$ as

$$\widetilde{\boldsymbol{C}} = \widetilde{\boldsymbol{R}}_{tx}^{T} \otimes \widetilde{\boldsymbol{R}}_{rx}, \tag{15}$$

where $\widetilde{\boldsymbol{R}}_{rx}$ and $\widetilde{\boldsymbol{R}}_{tx}$ are the $2 \times 2$ positive semidefinite Hermitian covariance matrices at the receive and transmit sides, respectively. Substituting (15) into (14), we can rewrite (14) as

$$\widetilde{\boldsymbol{H}}_c = \widetilde{\boldsymbol{R}}_{rx}^{1/2} \cdot \widetilde{\boldsymbol{H}}_w \cdot \widetilde{\boldsymbol{R}}_{tx}^{1/2}. \tag{16}$$

Based on (8), we can derive $\widetilde{\boldsymbol{R}}_{rx}$ and $\widetilde{\boldsymbol{R}}_{tx}$ respectively as

$$\widetilde{\boldsymbol{R}}_{rx} = E\left\{\widetilde{\boldsymbol{H}}_c \widetilde{\boldsymbol{H}}_c^{H}\right\} = \begin{bmatrix} 1 & \tilde{\rho}_{rx} \\ \tilde{\rho}_{rx} & 1 \end{bmatrix} \tag{17}$$

and

$$\widetilde{\boldsymbol{R}}_{tx} = E\left\{\widetilde{\boldsymbol{H}}_c^{H} \widetilde{\boldsymbol{H}}_c\right\} = \begin{bmatrix} 1 & \tilde{\rho}_{tx} \\ \tilde{\rho}_{tx} & 1 \end{bmatrix}, \tag{18}$$

where $\tilde{\rho}_{rx}$ and $\tilde{\rho}_{tx}$ represent the polarization correlation coefficients introduced to the small-scale fading components at the receive and transmit side, respectively. Experimental values of $\tilde{\rho}_{rx}$ and $\tilde{\rho}_{tx}$ are provided in [5], [11].

## IV. Algorithm for Modeling Dual-Polarized MIMO LMS Channel

Taking the channel effect analyzed in Section III into account, now we present Algorithm 1 as a practical method to model the dual-polarized MIMO LMS channel. At first, we input the state transition probability matrix $\boldsymbol{P}$, the current channel state $S_b$, the number of inner-loop iteration $M = \text{round}(L_f/L_m)$, and the number of outer-loop iterations $N = \text{round}(L/L_f)$, where $L$ is the travel distance of UT in meters. Then we initialize four channel vectors $\boldsymbol{h}_{ij}, i, j \in \{1, 2\}$ corresponding to four links of MIMO LMS communication systems. At each outer-loop iteration, we start by randomly generating a uniformly distributed random variable $u \sim U(0, 1)$ to simulate the random generation of different channel states including $S_1$, $S_2$ and $S_3$. Given the channel state, we determine $\alpha$, $\psi$ and $MP$ of Loo model from [7].

We use step 14 to step 25 to generate large-scale fading components of MIMO LMS channels. We initialize four channel vectors $\boldsymbol{g}_{ij}, i, j \in \{1, 2\}$ corresponding to the large-scale fading components of four links. Then we generate four

**Algorithm 1** Algorithm for Modeling Dual-Polarized MIMO Channel in LMS Communications

1: *Input:* $\boldsymbol{P}$, $S_b$, $N$, $M$.
2: *Initialization:* $\boldsymbol{h}_{ij} \leftarrow \boldsymbol{0}^{NM}, i, j \in \{1, 2\}$.
3: **for** $n = 1, ..., N$ **do**
4: Generate a random variable $u \sim U(0, 1)$.
5: **for** $i = 1, 2, 3$ **do**
6: $u_i = \sum_{j=1}^{i} p_{b,i}$.
7: **if** $u \leq u_i$ **then**
8: $S_b \leftarrow S_i$, Break.
9: **else**
10: $i = i + 1$.
11: **end if**
12: **end for**
13: Obtain $\alpha$, $\psi$ and $MP$ for $S_b$.
14: Generate initial phase $\phi_0 \sim U(0, 2\pi)$.
15: $\boldsymbol{g}_{ij} \leftarrow \boldsymbol{0}^{M}, i, j \in \{1, 2\}$.
16: Generate $\boldsymbol{g}_{ij}^{w} \sim \mathcal{N}(0, \boldsymbol{I}_M), i, j \in \{1, 2\}$.
17: Input $\boldsymbol{g}_{ij}^{w}$ to IIR filter, multiply the filter output with $\sqrt{1 - A^2}$, and obtain $\boldsymbol{g}_{ij}^{t}$, $i, j \in \{1, 2\}$.
18: **for** $m = 1, ..., M$ **do**
19: $\boldsymbol{G}^{t}(i, j) = \boldsymbol{g}_{ij}^{t}(m)$, $i, j \in \{1, 2\}$.
20: Obtain vec$(\boldsymbol{G}^{c})$ based on $\boldsymbol{G}^{t}$ according to (12).
21: Obtain vec$(\boldsymbol{G}^{\text{LN}})$ based on $\boldsymbol{G}^{c}$ according to (13).
22: $\boldsymbol{G}^{a} = \boldsymbol{G}^{\text{LN}} \odot \boldsymbol{G}^{p}$, where $\boldsymbol{G}^{p}$ is defined in (19).
23: vec$(\boldsymbol{G})$ = vec$(\boldsymbol{G}^{a})e^{j(\phi_0 + m\Delta\phi)}$ according to (6).
24: $\boldsymbol{g}_{ij}(m) = \boldsymbol{G}(i, j), i, j \in \{1, 2\}$.
25: **end for**
26: $\boldsymbol{q}_{ij} \leftarrow \boldsymbol{0}^{M}, i, j \in \{1, 2\}$.
27: Generate $\boldsymbol{q}_{ij}^{w} \sim \mathcal{CN}(0, \boldsymbol{I}_M)$, $i, j \in \{1, 2\}$.
28: Input $\boldsymbol{q}_{ij}^{w}$ to Butterworth filter, multiply the filter output with $B \times \sqrt{b_0}$, and obtain $\boldsymbol{q}_{ij}^{\text{R}}$, $i, j \in \{1, 2\}$.
29: **for** $m = 1, ..., M$ **do**
30: $\boldsymbol{Q}^{\text{R}}(i, j) = \boldsymbol{q}_{ij}^{\text{R}}(m)$, $i, j \in \{1, 2\}$.
31: Obtain vec$(\boldsymbol{Q}^{c})$ based on $\boldsymbol{Q}^{\text{R}}$ according to (14).
32: $\boldsymbol{Q} = \boldsymbol{Q}^{c} \odot \boldsymbol{Q}^{p}$, where $\boldsymbol{Q}^{p}$ is defined in (20).
33: $\boldsymbol{q}_{ij}(m) = \boldsymbol{Q}(i, j), i, j \in \{1, 2\}$.
34: **end for**
35: $\boldsymbol{h}_{ij}[(n-1)M + 1 : nM] = \boldsymbol{g}_{ij} + \boldsymbol{q}_{ij}, i, j \in \{1, 2\}$.
36: **end for**
37: *Output:* $\boldsymbol{h}_{ij}, i, j \in \{1, 2\}$.

vectors $\boldsymbol{g}_{ij}^{w}, i,j \in \{1,2\}$ with each entry of the channel vector obeying zero mean and unit variable Gaussian distribution. Each of $\boldsymbol{g}_{ij}^{w}, i,j \in \{1,2\}$ is passed through a low-pass IIR filter described in (4) to introduce temporal correlation, and then multiplied with $\sqrt{1-A^2}$ in amplitude to maintain the variance. The first inner-loop iterations from step 18 to step 25 introduce polarization correlation, shadowing effect, XPD effect and Doppler effect to large-scale fading components. In terms of XPD, we define $\boldsymbol{G}^{p}$ at step 22 to control the channel gain as

$$\boldsymbol{G}^{p} = \begin{bmatrix} \sqrt{1-\beta_{ant}} & \sqrt{\beta_{ant}} \\ \sqrt{\beta_{ant}} & \sqrt{1-\beta_{ant}} \end{bmatrix}. \tag{19}$$

We use step 26 to step 34 to generate small-scale fading components of MIMO LMS channels. We initialize four channel vectors $\boldsymbol{q}_{ij}, i,j \in \{1,2\}$ corresponding to the small-scale fading components of four links. Then we generate four vectors $\boldsymbol{q}_{ij}^{w}, i,j \in \{1,2\}$ with each entry of the channel vector obeying zero mean and unit variable complex-valued Gaussian distribution. Each of $\boldsymbol{q}_{ij}^{w}, i,j \in \{1,2\}$ is passed through a Butterworth filter described in (5) to introduce Doppler effect, and then multiplied with $B \times \sqrt{b_0}$ to maintain the variance and introduce multipath effect. The second inner-loop iterations from step 29 to step 34 introduce polarization correlation, XPD and XPC effect. We define $\boldsymbol{Q}^{p}$ at step 32 to control the channel gain as

$$\boldsymbol{Q}^{p} = \begin{bmatrix} \sqrt{1-\gamma} & \sqrt{\gamma} \\ \sqrt{\gamma} & \sqrt{1-\gamma} \end{bmatrix}. \tag{20}$$

At step 35, we combine the large-scale fading components $\boldsymbol{g}_{ij}, i,j \in \{1,2\}$ and small-scale fading components $\boldsymbol{q}_{ij}, i,j \in \{1,2\}$ together and finish one outer-loop iteration. After $N$ outer-loop iterations, the completely generated channel vectors $\boldsymbol{h}_{ij}, i,j \in \{1,2\}$ is finally output.

## V. Simulation Results

Now we simulate the channel model presented in Section IV. Suppose a UT moving at 10 m/s in three different environments, including open, suburban and urban environment. The working frequency is set to be 2.2 GHz at S band. The elevation angle $\theta$ and $L_f$ are set to be $40^\circ$ and 5 m, respectively.

For the Butterworth filter described in (5), we set the passband cutoff frequency to be $0.9v/\lambda$ at 3dB, and the passband cutoff frequency to be $3v/\lambda$ at 100dB. Then we can generate a $k = 7$th order Butterworth filter.

As shown in Fig. 2, we compare the channel state transition and the variation of the channel envelop for different environment. It is observed that as the UT moves, the channel state switches within three states. In the urban environment, the channel gain is smaller than that in the open environment because of the rich scatterers. Due to the effect of $XPD_{ant}$ and the $XPC_{env}$, the cross-polar channel envelope $|h_{ij}|, i \neq j$ is lower than the co-polar channel envelope $|h_{ij}|, i = j$.

We illustrate 1% outage capacity of the presented dual-polarized MIMO LMS channel through Monte Carlo simulations over $10^4$ channel realization in Fig. 3, Fig. 4, and Fig. 5 for different environments. Fig. 3 compares the 1% outage capacity for different $XPD_{ant}$ in open environment with fixed $\theta = 40^\circ$. It is seen that as $XPD_{ant}$ increases, the

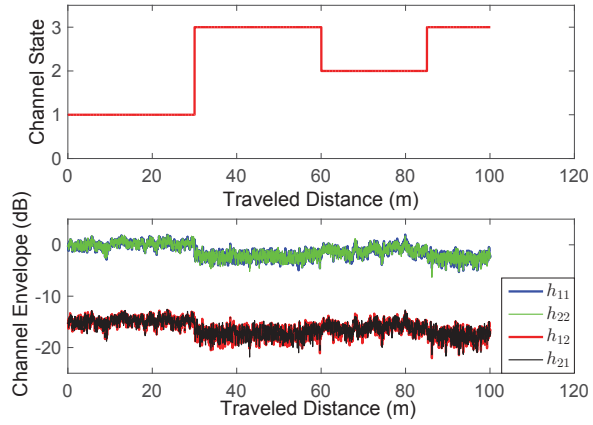


(a) Open environment

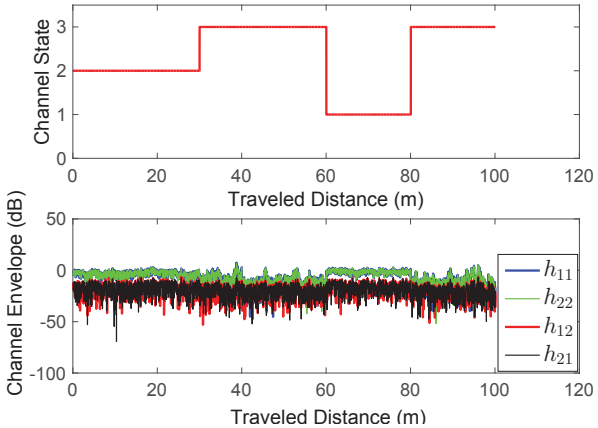


(b) Suburban environment

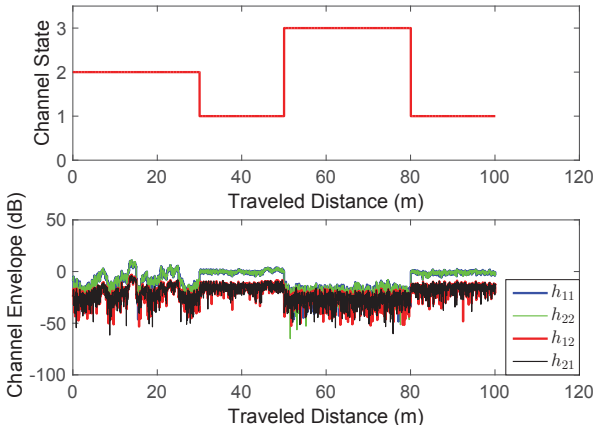


(c) Urban environment

Fig. 2. Generation of $2 \times 2$ dual-polarized MIMO LMS Channel for different environments.

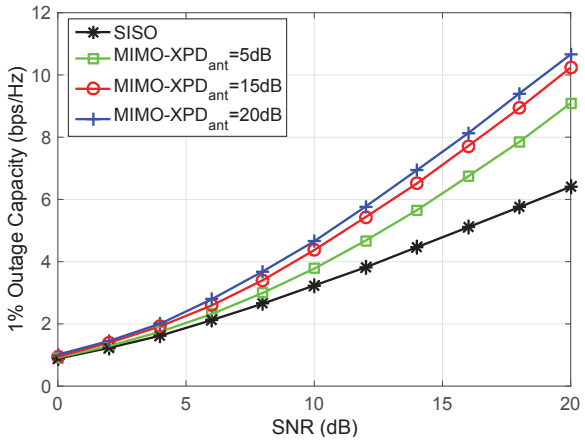


Fig. 3. 1% outage capacity of $2 \times 2$ dual-polarized MIMO LMS channel with the change of $XPD_{ant}$ in open environment ($\theta = 40°$).

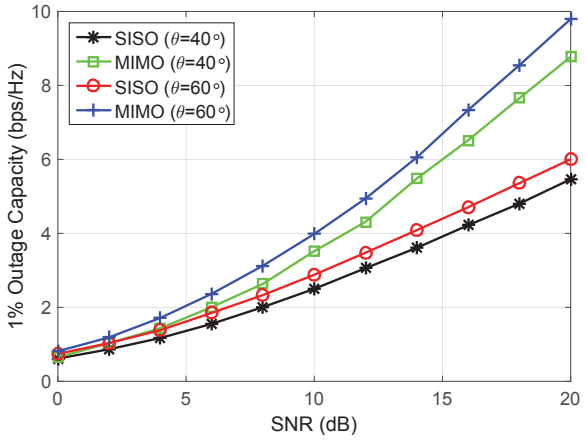


Fig. 4. 1% outage capacity of $2 \times 2$ dual-polarized MIMO LMS channel with the change of $\theta$ in suburban environment $XPD_{ant} = 15$ dB).

1% outage capacity also increases, since the cross polarization becomes weaker. Therefore, we may increase $XPD_{ant}$ of UT to reduce outage probability so that the system performance can be improved. Fig. 4 compares the 1% outage capacity for different elevation angle $\theta$ in suburban environment with fixed $XPD_{ant} = 15$ dB. It shows that with the increase of the elevation angle, the 1% outage capacity also increases, since the occurrence of $S_1$ among $S_1$, $S_2$ and $S_3$ becomes more frequent. Fig. 5 compares the 1% outage capacity for three different environments with fixed $\theta = 40°$.

It can be see from Fig. 3, Fig. 4, and Fig. 5 that the 1% outage capacity of MIMO channel is much higher than that of SISO channel. Given 20dB SNR, the 1% outage capacity of SISO channel in open, suburban and urban environment is 6.39 bps/Hz, 5.90 bps/Hz and 4.29 bps/Hz, respectively; whereas for MIMO channel, they are 10.63 bps/Hz, 9.42 bps/Hz and 6.59 bps/Hz, leading to the improvement of 66%, 60% and 54% for each environment.

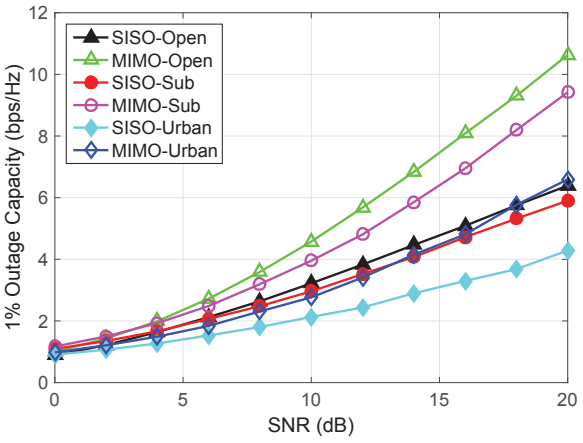


Fig. 5. 1% outage capacity of $2 \times 2$ dual-polarized MIMO LMS channel and SISO channel in open, suburban, urban environment ($\theta = 40°$).

## VI. Conclusions

In this paper, an algorithm has been presented to model dual-polarized MIMO LMS channel, which comprehensively investigates almost all factors, including temporal and polarization correlation, LOS shadowing, multipath effect, XPD of antennas, XPC of environments, elevation angle, user environments and Doppler frequency shift. Simulation results have shown that compared with SISO LMS system, MIMO LMS system can achieve significant improvement when measuring with 1% outage capacity.

## Acknowledgment

This work was supported in part by the National Natural Science Foundation of China under Grant 61302097, the Natural Science Foundation of Jiangsu Province under Grant BK20161428 and SAST2016072.

## References

[1] S. Fassoi, E. T. Michailidis, and A. G. Kanatas, "Performance evaluation of MIMO satellite multiple-relay multi-user fading channels," in *2015 9th European Conference on Antennas and Propagation (EuCAP)*, May 2015, pp. 1–5.

[2] P. Petropoulou, E. T. Michailidis, A. D. Panagopoulos, and A. G. Kanatas, "Radio propagation channel measurements for multi-antenna satellite communication systems: A survey," *IEEE Antennas Propag. Mag.*, vol. 56, no. 6, pp. 102–122, Dec. 2014.

[3] A. Byman, A. Hulkkonen, P. D. Arapoglou, M. Bertinelli, and R. D. Gaudenzi, "MIMO for mobile satellite digital broadcasting: From theory to practice," *IEEE Trans. Veh. Technol.*, vol. 65, no. 7, pp. 4839–4853, July 2016.

[4] C. Kourogiorgas, M. Kvicera, D. Skraparlis, T. Korinek, V. K. Sakarellos, A. D. Panagopoulos, and P. Pechac, "Modeling of first-order statistics of the MIMO dual polarized channel at 2 GHz for land mobile satellite systems under tree shadowing," *IEEE Trans. Antennas Propag.*, vol. 62, no. 10, pp. 5410–5415, Oct. 2014.

[5] P. King, "Modelling and measurement of the land mobile satellite MIMO radio propagation channel," *PhD Thesis, Univ. of Surrey*, 2007.

[6] K. P. Liolis, J. Gómez-Vilardebó, E. Casini, and A. I. Pérez-Neira, "Statistical modeling of dual-polarized MIMO land mobile satellite channels," *IEEE Trans. Commun.*, vol. 58, no. 11, pp. 3077–3083, Nov. 2010.

[7] F. P. Fontan, M. Vázquez-Castro, C. E. Cabado, J. P. Garcia, and E. Kubista, "Statistical modeling of the LMS channel," *IEEE Trans. Veh. Technol.*, vol. 50, no. 6, pp. 1549–1567, Nov. 2001.

[8] R. Prieto-Cerdeira, F. Pérez-Fontán, P. Burzigotti, A. B. Alamañac, and I. Sanchez-Lago, "Versatile two-state land mobile satellite channel model with first application to DVB-SH analysis," *Int. J. Satellite Communications Networking*, vol. 28, pp. 291–315, June 2010.

[9] P. R. King, T. W. Brown, A. Kyrgiazos, and B. G. Evans, "Empirical-stochastic LMS-MIMO channel model implementation and validation," *IEEE Trans. Antennas Propag.*, vol. 60, no. 2, pp. 606–614, Feb. 2012.

[10] V. Nikolaidis, N. Moraitis, and A. G. Kanatas, "Dual-polarized narrow-band MIMO LMS channel measurements in urban environments," *IEEE Trans. Antennas Propag.*, vol. 65, no. 2, pp. 763–774, Feb. 2017.

[11] P.-D. Arapoglou, K. Liolis, M. Bertinelli, A. Panagopoulos, P. Cottis, and R. De Gaudenzi, "MIMO over satellite: A review," *IEEE communications surveys & tutorials*, vol. 13, no. 1, pp. 27–51, First Quarter 2011.